Morphology and growth of metal clusters in the gas phase: A transition from spherical to ramified structures

R. Alayan, L. Arnaud, M. Broyer, E. Cottancin, J. Lermé, J. L. Vialle, and M. Pellarin*
Laboratoire de Spectrométrie Ionique et Moléculaire (U.M.R. CNRS 5579), Université Lyon1, Bât. A. Kastler, 43 Boulevard du 11 Novembre 1918, 69622 Villeurbanne Cedex, France
(Received 14 December 2005; published 30 March 2006)

Metal cluster cations are produced in a laser vaporization source, size selected in the gas phase by an electrostatic quadrupole deflector, and deposited without coalescence on carbon coated electron microscopy grids for further observation. For platinum clusters, a transition from spherical to strongly ramified shapes is observed when the cluster size increases beyond a critical diameter d_c of about 2.5 nm. In ramified structures, the branch width is almost independent of the size and of the order of d_c. This study shows evidence of the role of coagulation in the kinetics of growth and of the quenching of particle coalescence above the critical size. The results are discussed in the framework of previous models developed in aerosol and thin film growth experiments. A comparison with indium and gold clusters confirms that the border size at the transition from coalescence to ramification depends on the thermodynamic properties of the element.

DOI: 10.1103/PhysRevB.73.125444 PACS number(s): 81.10.Bk, 36.40.−c, 64.70.Nd, 61.46.−w

I. INTRODUCTION

A large interest is focusing on the individual and collective properties of supported size-selected clusters for both fundamental and technological purposes. One route is to synthesize deposits of clusters that are produced in the gas phase and delivered in a free propagating beam. Several techniques for an efficient size selection have been developed.[1–5] Since the size dependence of the cluster properties in the nanometer range is a key issue, additional parameters—such as their interaction with the substrate—must be controlled with care because they may blur intrinsic size effects. The properties strongly depend on the geometric structure and it is highly advisable to determine the cluster morphology prior to further analysis. The cluster shape is unfortunately governed by the kinetics of growth, and understanding how the cluster structure can deviate from compact arrangements is necessary before planning to control it by external means.

Most of the cluster sources work on the principle of condensing a supersaturated atomic vapor or plasma in an inert carrier gas. Beyond the characterization of size distributions,[6] mass spectroscopy experiments on cluster beams generated in such sources have provided valuable (although indirect) information about the geometrical structure of nanoparticles in the gas phase.[7,8] Generally speaking, clusters were found to adopt rather compact structures, indicating that they mainly grow by the addition of single atoms or small units.[9,10] Nevertheless, this is not the only mode of growth and the process of cluster-cluster coagulation may become important for other experimental conditions, systems, or even size ranges. This will be illustrated in the present paper and was clearly pointed out in pioneer experiments on aerosol particles produced in specially designed "inert-gas- evaporation" reactors.[11–13] Depending on the kinetics of rearrangement, this coagulation phase (also called agglomeration) may lead to compact, elongated, or dendritic shapes. Coagulation is naturally accounted for by conventional kinetic equations describing the growth of aerosols through sticking collisions between particles[14,15] but the issue of shape relaxation is more difficult to deal with. The recent molecular dynamics study of Meyer *et al.*[16] on nickel particles illustrates an interesting attempt to describe the interplay between both processes.

The formation of highly ramified or fractal particles in conventional cluster beam generators has not been investigated in detail up to now. The in-flight characterization of cluster morphologies is difficult even if their mass is sharply selected. As compared to spherical particles, deformed ones could lead to different responses in light scattering[17] or ion mobility measurements[18] for instance, but rotational averaging effects prevent their shape from being determined unambiguously. On the other hand, a few microscopic studies of clusters synthesized in the gas phase and deposited on surfaces have directly and unambiguously shown the existence of deformed and ramified structures.[13,19] These are not stable on thermodynamical grounds but their coarsening dynamics towards a compact shape is slow compared with the observation time window (delay between cluster synthesis and shape characterization).

In the absence of a precise mass selection, the relation between size and shape is hindered by a residual growth on the surface because of cluster diffusion and collision. Observed and incident particles may be different. We have recently developed an experimental setup for the synthesis of supported assemblies of size-selected clusters. The sharp size distribution of deposited particles gives the opportunity to unambiguously correlate their size to their geometrical structure in the gas phase. After discussing this point, we present the experimental evidence that coagulation events are of main importance in the cluster growth from a laser plasma quenched in an inert carrier gas atmosphere (standard laser vaporization source). In the case of platinum, a transition from spherical to ramified clusters is clearly observed and we discuss the shape of large dendritic structures as resulting from a size-dependent competition between coagulation and coalescence processes. A comparison with indium and gold

clusters confirms the importance of the thermodynamical properties of the element with respect to this competition.

II. EXPERIMENT

Metal clusters are produced in a laser vaporization source at room temperature. The charged species present in the beam effusing from the source are deviated at right angle and energy selected by an electrostatic quadrupole. Because the cluster velocity is rather well defined and almost independent of the size, the filtering of kinetic energy is an efficient means to sharpen the size distribution in the beam. Detailed information about the operation and the performances of the whole setup is available in a previous publication.[5] The aim of this paper is to illustrate how the morphology of metal clusters evolves as a function of size. We will mainly focus on the special case of platinum clusters. Here, we opt to deposit size-selected clusters on a surface (amorphous carbon film) by means of the LECBD (low energy cluster beam deposition) technique.[20] They are further observed and characterized by transmission electron microscopy (TEM). They may be slightly deformed because of collision and interaction with the substrate but one can nevertheless retrieve valuable information about their morphology prior to deposition, as will be discussed in the next section.

Before discussing TEM images, let us recall that their examination gives only access to the projected shape of clusters deposited on the substrate surface. Since the cluster cross profile in the direction perpendicular to surface is unknown, the measurement of the projected area S_p is not sufficient to obtain a precise estimate of the cluster volume, especially in the case of very deformed particles. In the so-called spherical approximation, an "effective radius" r_{eff} is given by $S_p = \pi r_{eff}^2$. The effective cluster volume $\mathcal{V}_{eff} = \frac{4}{3}\pi r_{eff}^3$ is the real one only when clusters are perfectly spherical (no surface wetting or oblate deformation). The cluster size (i.e., volume) is a central parameter that must then be controlled by other means. When the four quarter cylindrical electrodes of the quadrupole are alternately polarized with a static $\pm V$ bias, the mean kinetic energy of right-angle deviated clusters is $E_c = eV$ (e is the elementary electric charge) and their mass is $m = 2eV/v_o^2$ since the bulk of ionized clusters are singly charged. The selection of kinetic energy provides a direct measurement of the mass provided that the cluster velocity v_o is known. In our laser vaporization source, v_o has proven to depend mainly on the expansion conditions (gas pressure, nozzle diameter) but not on the constituting element. As a consequence, the particles will be always produced under similar expansion conditions. This ensures that the proportionality factor between mass and kinetic energy is fixed and remains unchanged throughout the experiment.

Here, v_o was measured by a time of flight technique and found close to 570 m/s for the most abundant species ($E_c = 150-200$ eV).[5] Strictly speaking, the actual cluster velocity is not exactly constant and a slight slippage (decreasing velocity with increasing size) must be considered. A direct measurement was not performed here. A further study on supported spherical indium clusters has shown that a lowering of 10% relative to v_o can be considered as an upper value for the largest sizes ($E_c = 1200$ eV).[5] This effect is weak and the approximation of a constant velocity does not alter the main conclusions of this study, as will be illustrated in the next section.

III. RESULTS

The micrographs in Fig. 1 show deposits of platinum clusters of three different kinetic energies $E_c = 140$ eV, 300 eV, and 1200 eV. Assuming a size independent velocity $v_o \cong 570$ m/s, they contain respectively $N = 420$, 900, and 3600 atoms on the average. The coverage rate was monitored during the deposition process by measuring the cumulated charge impinging on the grid surface [10 nC for Figs. 1(a) and 1(b) and 1 nC for Fig. 1(c)]. A charge of 1 nC corresponds to a particle density of the order of 5.10^{10} cm^{-2}. As the size increases, the morphology of deposited clusters strongly changes from spherical to elongated and finally strongly distorted shapes.

The important point is that the individual particles that can be identified in the TEM images, with a few exceptions, are not the result of the merging and reorganization of several incident ones. The coverage rates measured from the micrographs are indeed close to the values inferred from cumulated electric charge measurements in the case of singly ionized particles [3×10^{11} cm^{-2}, 4.5×10^{11} cm^{-2} and 0.8×10^{11} cm^{-2} for Figs. 1(a)–1(c) respectively]. Additional arguments support the absence of a significant amount of particle diffusion and regrouping on the surface. Clusters selected at $E_c = 140$ eV kinetic energy ($N = 420$) were previously analyzed in Ref. 5. Their diameter distribution was deduced from the histogram of projected surfaces [Fig. 1(a)] by assuming the spherical approximation. The mean diameter $\bar{d} \cong 2.30$ nm ($\bar{S}_p = \pi(\bar{d}/2)^2 = 4.2$ nm^2) is exactly the one predicted for particles with 140 eV kinetic energy, which is in favor of the spherical shape and the absence of cluster agglomeration on the substrate. For larger and no longer spherical particles, the only relevant quantity to be considered is their projected surface. In the case of $N = 900$ [Fig. 1(b)] and 3600 atom clusters [Fig. 1(c)], the relative surface dispersion is surprisingly low ($\Delta S/\bar{S} \cong 34-38\%$) and of the same order as for $N = 420$ atom clusters. The nonmeasurable cluster height is certainly not less precisely defined for $N = 900$ and $N = 3600$ than for $N = 420$ atom clusters. In this case, the relative volume dispersion $\left[\Delta\mathcal{V}/\bar{\mathcal{V}} \cong \frac{3}{2}(\Delta S/\bar{S}) \cong 55\%\right]$ is almost independent on the size and remains close to the selectivity of the quadrupole deviator,[5] smaller than the island size dispersion that would be expected for a ballistic and random deposition process followed by cluster diffusion and regrouping.

If particle diffusion and sintering on the surface do not significantly contribute to the morphology of cluster deposits, the one-to-one correspondence between incident and supported particles can still be hindered by fragmentation events. Since the clusters are not decelerated before impinging on the surface, a part of their kinetic energy is available

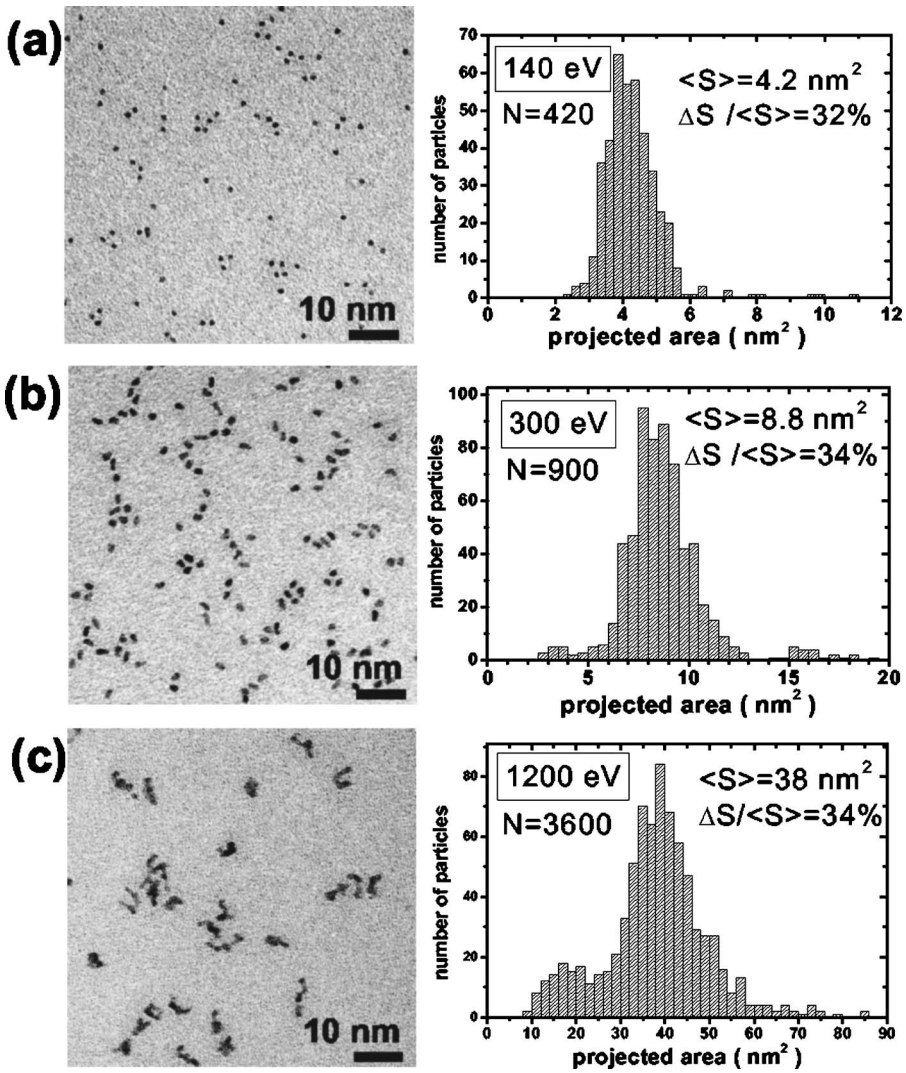

FIG. 1. Transmission electron micrographs and projected surface histograms of size selected platinum clusters deposited on amorphous carbon. The selected kinetic energies are (a) 140 eV, (b) 300 eV, and (c) 1200 eV corresponding to $N=420$, 900, and 3600 atom clusters respectively.

for further warming and reorganization. As a general rule, the kinetic energy per atom is a constant that only depends on the initial cluster velocity. It is of the order of 0.33 eV in the case of platinum. This is much less than the cohesive energy per atom [5.84 eV (Ref. 21)] which makes the atomic evaporation process unlikely. On the other hand, if the particles are ramified and built by the attachment of a few smaller entities, an excess energy can more likely induce the breaking of interparticle links if it is localized in the corresponding vibrational dissociation modes. This is obvious in the case of the largest clusters [Fig. 1(c)] for which a shoulder is detected on the left side of the surface distribution.

To disclose more clearly the shape evolution of platinum clusters with size, Fig. 2 shows enlarged views of selected particles deposited with various kinetic energies E_c $=100$ eV, 140 eV, 300 eV, 800 eV, 1000 eV, and 1200 eV. The corresponding average sizes are respectively $N=300$, 420, 900, 2400, 3000, and 3600 atoms ($v_o \cong 570$ m/s). For $N=300$ and 420 atoms, the clusters appear spherically shaped even if crystalline facets can be guessed under larger magnification. For $N=900$, the most abundant shape is now close to a prolate ellipsoid with a visibly well-defined eccentricity $e=0.83\pm0.06$. The average lengths of the long and short axes are about 4.5 nm and 2.5 nm respectively. The short axis is hardly larger than the diameter of the spherical $N=420$ atom clusters. When their size is increasing, the clusters become more and more deformed. Particles with N $=900$ atoms are not elongated in a single direction but present an outset of branching which is magnified for larger particles containing $N=2400$, 3000, and 3600 atoms. In the last case, it was possible to identify a very few spherical particles, such as the one displayed in Fig. 2. The main feature is the constancy of the branch width of ramified particles ($\cong 2.5$ nm). It is similar to the short axis length of the prolate particles selected at 300 eV ($N=900$) and appears as a characteristic length for the lateral extension of particle arms in the plane of the substrate.

As mentioned in the previous section, the volume of deformed clusters cannot be directly measured from TEM images. In Fig. 3, the apparent area S_p of three cluster sizes (see Fig. 1) is plotted as a function of the cluster kinetic energy ($E_c=140$ eV, 300 eV, and 1200 eV). The selected clusters are expected to contain, on the average, $N=420$, 900, and 3600 atoms which correspond, for platinum, to the respective volumes $\mathcal{V}=6.35$ nm^3, 13.61 nm^3, and 54.43 nm^3 [atomic mass 195.1 amu and bulk density 21.4 g/cm^{-3} (Ref. 21)]. If

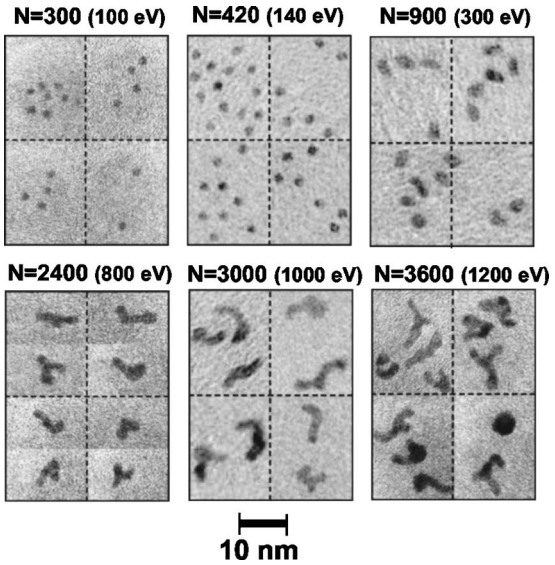

FIG. 2. Enlarged micrographs of selected clusters deposited with various kinetic energies: $E_c=100$ eV ($N=300$), $E_c=140$ eV ($N=420$), $E_c=300$ eV ($N=900$), $E_c=800$ eV ($N=2400$), $E_c=1000$ eV ($N=3000$), and $E_c=1200$ eV ($N=3600$). The bottom rightmost picture displays a spherically shaped particle with $N=3600$ atoms.

the clusters were spherical, the points should scale as $E_c^{2/3}$ since $S=\pi[(3/4\pi)\mathcal{V}]^{2/3}$ ($\mathcal{V}$ is proportional to E_c) and should fall onto the dotted line in Fig. 3, at the corresponding abscissas $S_p=4.15$ nm^2, 6.89 nm^2, and 17.34 nm^2. This is verified both for the $N=420$ atom clusters and the compact $N=3600$ atom cluster visible in the bottom right-hand corner of Fig. 2. On the contrary, the projected areas for $N=900$, and $N=3600$ are much larger than expected and rather scale as E_c. This is an indication that ramified clusters have almost a constant height. If S_p is the projected area of a spherical particle with volume $\mathcal{V}$ and diameter $D=\frac{3}{2}(\mathcal{V}/S_p)$, $\mathcal{V}$ can be also expressed as $\mathcal{V}=\epsilon S_p$ where $\epsilon=\frac{2}{3}D$ can be seen as an effective thickness (height of a cylinder of section S_p and with the same volume). This also holds for an ellipsoid of revolution. Let us assume that the ramified particles remain planar over the substrate and that their real height can also be written $H=\frac{3}{2}(\mathcal{V}/S_p)=\frac{3}{2}\epsilon$. We find $H=2.3$ nm and $H=2.15$ nm for $N=900$ and $N=3600$ atom clusters. This confirms indeed that the particle extension perpendicular to the substrate is almost constant and close to the characteristic branch width in the plane of the substrate ($H\cong d_c$). Platinum clusters are likely to adopt a dendritic shape with branches that have similar and size-independent extensions both parallel and perpendicular to the substrate. Therefore, their volume is almost proportional to the cumulated length of these branches, as can be guessed from TEM images. It must be noted that if a weak velocity slip were no longer neglected (see Sec. II), the dotted curve in Fig. 3 would be slightly distorted and, in the vicinity of $E_c=1200$ eV, shifted about 13% towards higher S_p values. This corresponds to an increase of about 7% of the H value inferred for $N=3600$. This correction is weak and H remains consistent with expectations. The hypothesis of a constant velocity is therefore acceptable.

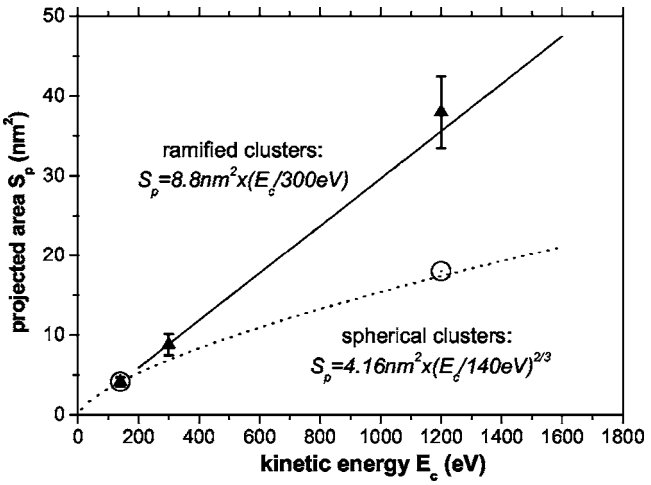

FIG. 3. Plot of the average projected area S_p as a function of the cluster kinetic energy E_c, for the three size histograms reported in Fig. 1 (▲). The circles (○) correspond to the special values of the particles in Fig. 1(a) ($E_c=140$ eV, $N=420$) and the spherical isolated particle in Fig. 2 ($E_c=1200$ eV, $N=3600$). The dotted curve gives the evolution of S_p if the particles were all spherically shaped. The full line illustrates the case of a linear dependence of S_p with E_c and is arbitrary scaled with the point measured at $E_c=300$ eV ($N=900$).

IV. DISCUSSION

A. Cluster growth through coagulation

Whatever the method for creating the initial atomic vapor (thermal evaporation, laser ablation, ion sputtering, etc.), the synthesis of nanoparticles in the gas phase starts with a nucleation stage where the vapor, usually supersaturated in an ambient inert gas atmosphere, rapidly condenses into small primary particles. Once most of the atomic species are depleted, the prevailing mechanism becomes the attachment of colliding clusters starting from those primary particles (coagulation stage). Under the hypothesis of irreversible aggregation, the temporal evolution of the cluster size distribution is described by the standard coupled kinetic equation system[22]

$$\frac{dX_n(t)}{dt}=\frac{1}{2}\sum_{i+j=n}\kappa_{ij}X_i(t)X_j(t)-X_n(t)\sum_{i\geqslant 1}\kappa_{in}X_i(t), \quad (1a)$$

where $X_n(t)$ is the number of clusters per unit volume with n atoms at time t and the κ_{ij} kernels give the collision rate of clusters containing i and j atoms. Coagulation has proven to be of main importance in most of the cluster sources. The size distributions usually disclose a practically log-normal profile, as is expected if this mechanism prevails (see Appendix A).[6] Moreover, coagulation is also a prerequisite for the growth of noncompact shapes. Generally speaking, clusters result from a sequence of binary sticking collisions to which their final size and morphology will be extremely sensitive (see notations in Appendix B).

In the following, it will be useful to make a comparison with a well-known but somewhat different mechanism. It concerns the growth of nanostructured agglomerates on surfaces by depositing size selected clusters ($n=n_o$), preformed in the gas phase and delivered in the form of a molecular beam.[23–25] Soft-landed clusters undergo Brownian diffusion on the slippery substrate until they impinge onto motionless islands or trapping defects. Here, the kinetics of two-dimensional growth can be simplified and described by the equation

$$\frac{dX_n(t)}{dt} = k_{n-n_o,n_o} X_{n-n_o}(t) X_{n_o}(t) - k_{n,n_o} X_n(t) X_{n_o}(t). \quad (1b)$$

The size dependence of the collision frequencies can be neglected ($k_{j,no}=k=1/\Delta t_{col}$) in a first approximation. $1/\Delta t_{col}$ is roughly proportional to the intensity of the primary cluster beam that is assumed to be constant [constant $X_{n_o}(t)$]. The total amount of matter is only limited by the duration of the deposit.

B. Limited sintering and ramification

Considering either gas phase or surface growth conditions, the sequential sticking of building particles at different places (coagulation) produces a progressive spread and branching of a growing cluster island, whereas sintering and coalescence drive its coarsening towards a larger compactness. The final morphology results from a subtle balance between these two conflicting mechanisms. Relaxation through coalescence is usually pictured in the simplest case of spherical clusters (radii r and R). The most stable structure is obtained when both particles merge to form a single, spherically shaped entity. Several processes of matter transport are involved during sintering and coalescence but surface diffusion is known to be of main importance on the nanometric scale.[26] The neck between particles is a region of locally low curvature towards which the surface atoms are likely to migrate so as to reinforce atomic bounds. Whatever the nature of the dominant contribution to coalescence, its dynamics is ruled by a characteristic time $t_s(r,R,T)$ which is a rapidly increasing function of the particle radii at fixed temperature T.[25,27]

When coalescence is much faster than the delay Δt_{col} between successive arrivals of colliding clusters ($\Delta t_{col} \gg t_s$), the particle has time to evolve into a fully compact (spherical) shape at any step of the growth. On the contrary, if coalescence is so slow that it can be neglected on the time scale of growth ($\Delta t_{col} \ll t_s$), individual clusters attach without sintering. In the final particle, the primary clusters remain identifiable within the "pearl-like" branches of the "fractal-like" skeleton and the memory of their structure is preserved. In ordinary growth conditions, an intermediate situation takes place ($\Delta t_{col} \cong t_s$). A colliding cluster c partly merges into a growing island C until a further sticking event will freeze this process or slow it down beyond the observation time window. This is the key point of particle shaping. Except for a sudden cooling of the condensing vapor, it consists in the attachment of a third cluster c' to the coalescing pair c-C and the formation of a second neck, as illustrated in Fig. 4. When their sizes are clearly different and under the hypothesis of a surface diffusion mechanism for coalescence, the merging of c into C will be all the more slowed down if c' impinges on the c-C system in the vicinity of c. The maximum effect is obtained when c is sandwiched between C and c' since its surface atoms are drawn in opposite directions towards the c-C and c-c' necks. Such an event actually proves to rule the degree of particle coarsening.

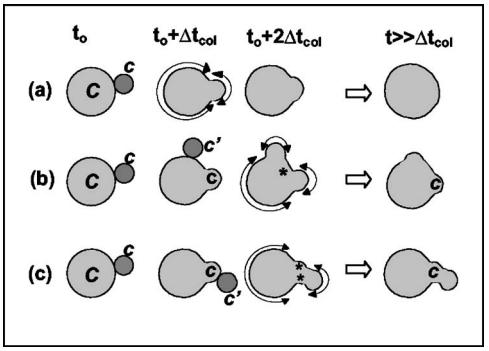

FIG. 4. Qualitative evolution of a growing cluster shape after the collision with one or two primary clusters. Δt_{col} is a characteristic collision time interval. The arrows indicate the net displacement of diffusing surface atoms: (a) if only one collision occurs, cluster c will progressively merge into C to give a single, nearly spherical particle at time t, (b) a second cluster c' collides onto C. The dissolution of c into C is slowed down and not complete at time t. The star indicates the region of the surface where the atoms can now diffuse towards two neck regions, (c) the second cluster c' collides onto c. The dissolution of c into C is frozen since its surface atoms have additional high curvature regions to fill up.

It must be noticed that if Δt_{col} is the mean delay between successive collisions at any point of the outer surface of the growing island C, the delay $\Delta^* t_{col}$ between the arrival of a primary cluster c on the main particle C and the collision of a next one c' onto c will be larger. It can be roughly written $\Delta^* t_{col} \cong \mathrm{a}.\Delta t_{col}$ with $\mathrm{a}=S/[\pi(r^*+r')^2]$ or $\mathrm{a}=L/[2(r^*+r')]$ for gas phase or surface growth respectively (S is the surface of the island envelope, L is the island periphery in the substrate plane, r' is the radius of the c' cluster and r^* is the apparent radius of the coalescing cluster c at the moment of the collision). Δt_{col} can be calculated from suitable collision kernels even if colliding clusters have distorted shapes[12] but it is difficult to estimate precisely $\Delta^* t_{col}$ that is the delay of interest. In any case, $\Delta^* t_{col} \cong \Delta t_{col}$ in the earliest stages of growth whereas $\Delta^* t_{col} \gg \Delta t_{col}$ when growing islands are very large as compared to primary particles. The slowing down of coalescence of c by the influence of a third cluster c' does not exclusively proceed in the situation depicted in Fig. 4(c) but a sufficient proximity of c and c' [as in Fig. 4(b)] gives almost similar results. The role of c' is ineffective when c and c' are located at distant places of the periphery of a large island. Since the sizes of c and C clusters are not very different in Brownian coagulation,[14] we will make here the assumption that $\Delta^* t_{col}$ always remains close to Δt_{col}, which will be considered as the effective collision time interval, at least for gas phase growth.

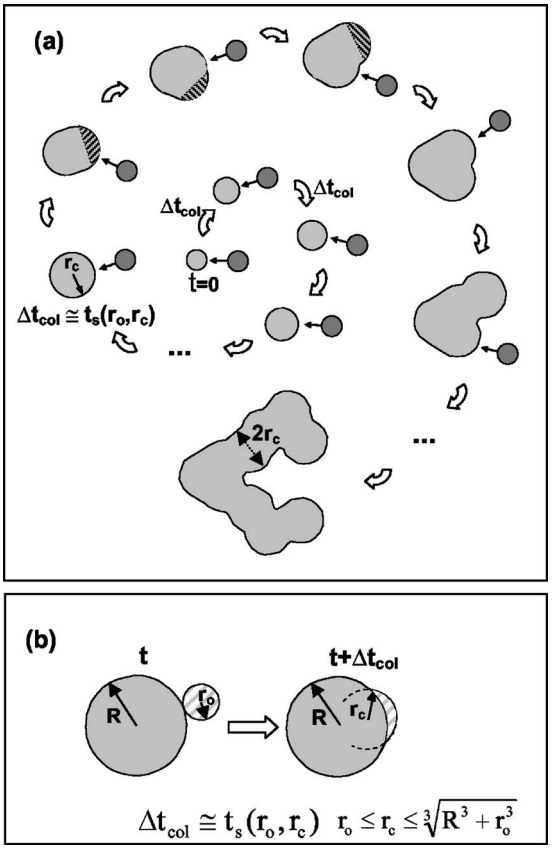

FIG. 5. (a) Schematic growth of a ramified particle with a $2r_c$ branch width, from the successive attachment of identical clusters (dark gray spheres with radius r_o). The characteristic time $t_s(r_o,r_c)$ for the coalescence of spheres with radii r_o and r_c is of the order of the mean collision time interval Δt_{col}. (b) Graphical method to approximate the overall shape of a dissymmetrical pair of initially spherical clusters. The colliding cluster (the smallest one) is supposed to change its shape from a complete sphere with radius r_o to a truncated sphere of radius r_c such as $t_s(r_o,r_c) \cong \Delta t_{col}$.

The simplest case of primary particles having the same radius r_o and colliding regularly in the same region of the growing seed is illustrated in Fig. 5(a). Between successive collisions, the growing particle retains a spherical shape until its size reaches a critical radius r_c for which

$$t_s(r_o,r_c,T) \cong \Delta t_{col}. \tag{2}$$

From that time, the particle is too large to allow a complete assimilation of the primary clusters and does not remain spherical any longer, since beyond the characteristic radius r_c one has $t_s(r_o,r>r_c,T)>\Delta t_{col}$. The concept of a *local radius* (or local curvature) at the contact point will be more relevant to estimate the characteristic time for coalescence t_s and to infer the shape relaxation between further attachments. Even macroscopic theories are not able to fully describe the incomplete merging of the cluster pair after this transition time. It can be nevertheless predicted that, between successive collisions at any point of the particle surface, the sintering and neck growth will be quenched in surface regions having a local curvature lower than the limiting value $1/r_c$. This dynamics is schematized in Fig. 5(a) and results in the formation of ramified particles with calibrated branches having a mean width close to the critical diameter $d_c=2r_c$. If one is more interested in the overall cluster shape than the exact neck geometry, Fig. 5(b) shows a crude but practical method for defining the outer envelope of a coalescing pair of spheres as a function of time. This easy graphical representation is consistent with the description of Fig. 5(a) and will be used in the following.

C. Dendritic clusters in the gas phase: An analogy with surface growth mechanisms

The previous description was developed by Yoon *et al.* in their study of supported islands grown from antimony clusters soft-landed onto graphite.[25] The size and the beam intensity of primary clusters are sharply defined. The mean collision time is not strictly proportional to the inverse beam intensity but corrected to account for the increase in the island periphery as the growth is proceeding (see Sec. IV B). The increase with time is slow as compared to coalescence dynamics and the qualitative conclusions remain valid if the collision time is set strictly constant. This explains the growth of fractal-like structures with a uniform branch width $d_c \cong 2r_c$ in agreement with the representation of Fig. 5(a). At first sight, the resemblance to our observations on platinum clusters is surprising owing to the differences between growth processes. Gas phase growth has been widely studied in the framework of kinetic equations as (1a), especially under the hypothesis of an isothermal and Brownian coagulation in the free molecular regime.[6,14,15,28–30] The cluster size distribution is approximated by a stable "self-preserving distribution" (SPD) as summarized in Appendix A. Contrary to the average size of colliding clusters, the particle density and so the collision frequency decrease with time because the available amount of matter is constant and fixed by the number of initially vaporized atoms. This is different from deposition experiments.[25] Obtaining ramified particles with uniformly sized branches would mean that an increase in the collision time Δt_{col} is almost offset at each collision step by a corresponding increase in the coalescence time in such a way that relation (2) remains fulfilled for a constant r_c value.

Understanding the onset of ramification requires a reliable formulation of both the kinetics of growth and the coalescence dynamics. If the first one can be modeled without too much difficulty (Brownian coagulation in the gas phase[14] or diffusion limited aggregation models for surfaces[23]), an accurate treatment of the second issue is very difficult and must account for various factors and for the specific element studied. Qualitative but acceptable information can nevertheless be obtained provided that the characteristic time for coalescence can be handled through an analytical scaling law. We choose the approximate but general form

$$t_s(r,R,T) = A(T) r^{\alpha} R^{\beta}, \tag{3}$$

where $A(T)$ is an adjustable parameter depending on the temperature. In the following, we will set $\alpha=\beta=2$ which has advantage fitting with the analytical formula of macroscopic

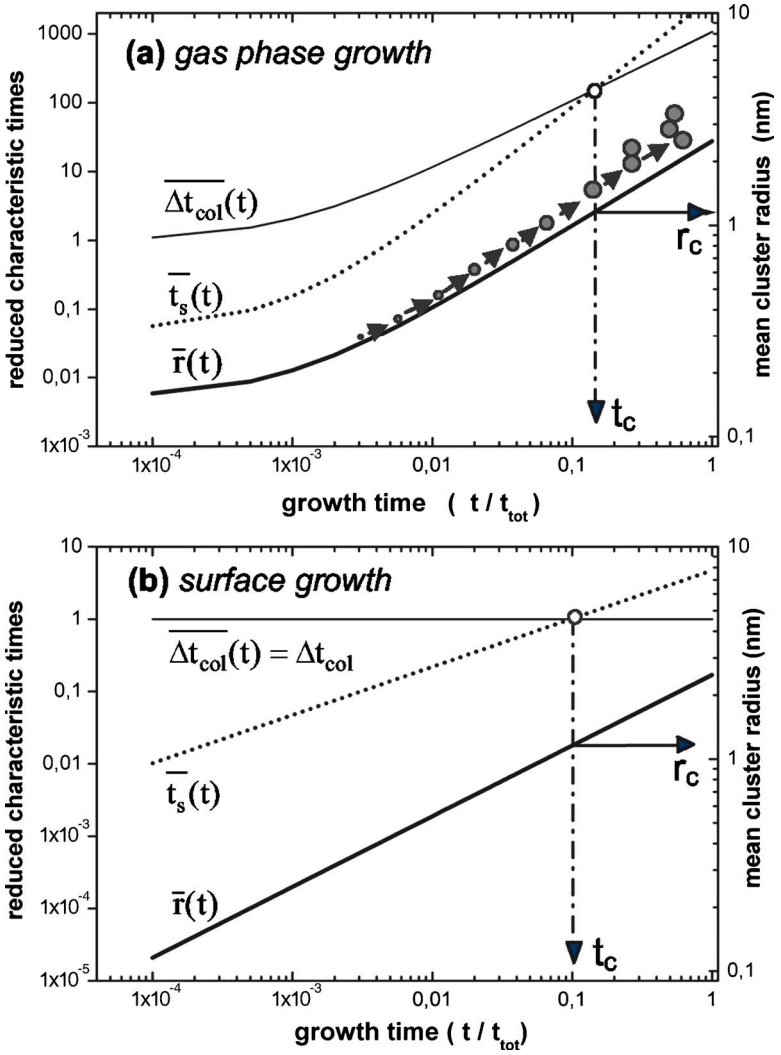

FIG. 6. (Color online) Time dependence of the average cluster radius and the characteristic times for collision ($\overline{\Delta t_{col}}$) and coalescence ($\overline{t_s}$) in the case of: (a) gas phase growth (see Appendix A), and (b) surface growth. In (b), the incident cluster size (n_o=50) is chosen in such a way the final mean cluster radius and the critical radius r_c are the same as in (a). The use of a reduced time of growth t/t_{tot} makes the determination of the cluster beam intensity superfluous. The value $A(T)/t_{tot}=3.310^{-2}$ nm^{-4} was used in both cases. The characteristic times are normalized by $\Delta t_{col}(t=0)$ and the cluster radii are effective values obtained by assuming spherical shapes.

theories for both usual cases: $r=R$ and $r=r_o \ll R$.[25,31]

Experiments deal with large cluster assemblies for which only average quantities (sizes and collision times) are relevant. Flagan and Lunden have therefore proposed a general scheme to explain the formation of ramified particles in the gas phase.[12] At each time of the growth stage, they have considered the average size $\bar{n}(t)$ [average volume $\bar{v}(t)$] of the actual cluster distribution (self-preserving distribution) as the characteristic size of colliding particles. An instantaneous characteristic time for collision is taken as the average value $\Delta t_{col}^{\mathrm{SPD}}(t)$ that can be defined in the framework of the SPD approximation (A2). The characteristic time for coalescence $t_s(t)$ is associated to the merging of two identical clusters $C_{\bar{v}(t)}$ and is given by $t_s(t)=A(T)\bar{r}^4(t)$ according to relation (3) [$\bar{r}(t)$ is the average cluster radius]. If the condition $t_s(t)=\Delta t_{col}^{\mathrm{SPD}}(t)$ is fulfilled at a time $t=t_c$, it can be roughly argued that the coalescence of colliding clusters is complete before t_c and frozen after. As a consequence, clusters smaller than $\bar{v}(t_c)$ are spherical when larger ones are ramified and made by the attachment of intact units with volume $\bar{v}(t_c)$. This description is illustrated in Fig. 6(a) for a choice of SPD parameters accounting for the cluster size distribution observed in the experiment (Appendix A). The parameter $A(T)$ is adjusted to bring the critical size $r_c=\bar{r}(t_c)$ close to the half branch width of platinum clusters in Fig. 2 [$A(T)/t_{tot}=3.310^{-2}$ nm^{-4} and t_{tot} is the total time allocated for growth]. In this scheme, a strong divergence between $t_s(t)$ and $\Delta t_{col}^{\mathrm{SPD}}(t)$ on both sides of t_c is also invoked so as to inhibit a further neck growth.

This appealing description qualitatively accounts for the average morphology of particles grown from inert gas condensation reactors.[11,12] It matches the present experimental observations although it is first intended to provide average information on size dispersed cluster assemblies. In this framework, it is not possible to explain the weak dispersion of branch widths as a function of cluster size (see Fig. 2). Instead of discussing the cluster ramification in terms of the mean size properties, we go a little further by considering a *particular* size N observed at time t_{tot} and by choosing to construct an "average history" of its growth in the form of a stepwise sequence (Appendix B). We have first applied this method to surface growth in deposition experiments (incident clusters with n_o atoms). The results for two selected sizes are illustrated in Fig. 7. For surface growth and thanks to the crude approximations made, an analytical calculation is possible which makes the description of the results simpler [see Eq. (1b)]. Whatever the final size N, the average colli-

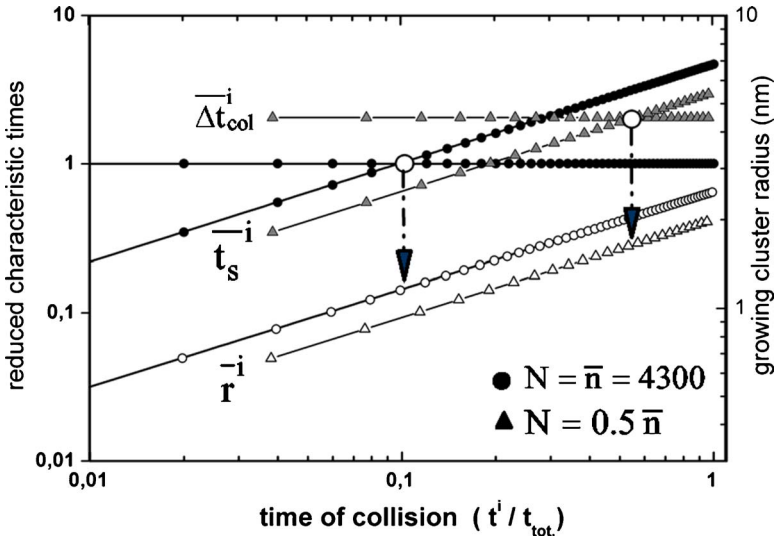

FIG. 7. (Color online) Average sequences for the formation of clusters containing $N=\bar{n}(t_{tot})=4300$ (circles) and $N=0.5\bar{n}(t_{tot})=2150$ atoms (triangles), in the case of surface growth and with the same ingredients as in Fig. 6(b). The different points give the average values of the characteristic times for collision and coalescence (full symbols) and the average equivalent radius of the growing island (empty symbols) as a function of the successive reduced times of collision t^i/t_{tot}. t_{tot} is the total time of growth and the characteristic times are all normalized by the particular value $\overline{\Delta t_{col}}(t=0)$ obtained for $N=\bar{n}(t_{tot})=4300$. Full and dotted lines are drawn for guiding the eyes. The intersections between $\overline{\Delta t_{col}}$ and $\bar{t}_s^i$ curves indicate the critical radii or half of the branch widths.

sion time is time independent and can be expressed as $\overline{\Delta t_{col}}=t_{tot}\frac{n_o}{N}$. The critical radius r_c that fulfills $t_s(r_o,r_c,T)\cong\overline{\Delta t_{col}}$ can be written $r_c=r_o^{-1}\sqrt{\overline{\Delta t_{col}}/A(T)}\propto 1/\sqrt{N}$ and is indeed a decreasing function of N (see Fig. 7). This is confirmed in Fig. 8, which displays a graphical representation of simulated growth sequences and final branch widths for different cluster sizes. These drawings do not represent real particles but rather the evolution of their outer envelope that develops in the course of growth by assuming that the flux of colliding clusters propagate along a single direction. The simplified representation of a "linear growth" is valid only because the effective collision rate on a given particle has been supposed to be independent on the exact location of the collision at its surface (Sec. IV B).

The dispersion of branch widths about the average value that can be guessed from Fig. 7 is also noticeable in Fig. 8. The case of gas phase synthesis deserves to be discussed

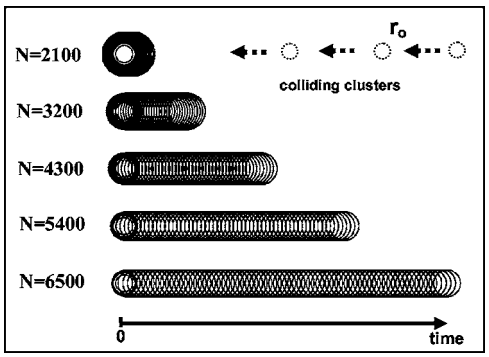

FIG. 8. Simulated time evolution of the branch width for several selected particles, on the basis of calculated surface growth sequences (see Fig. 7, for instance) and using the graphical method explained in Fig. 5(b). The particle outer envelope develops along a single direction, from left to right, by assuming that successive collisions occur on the right side of the growing islands. As long as the coalescence time is shorter than the collision time, the particles coalesce and grow spherical until the situation is reversed and the branch width stabilized to a constant value. The incident cluster radius r_o is indicated as a reference.

from this angle and Fig. 9 shows the calculated average sequences for the growth of two sizes ($N=900$ and $N=4300$) through Brownian coagulation in the gas phase. We first explore the case of an isothermal growth with the previous value $A(T)/t_{tot}=3.10^{-2}\ \mathrm{nm}^{-4}$. The curves for collision (empty squares) and coalescence times (full triangles) do not display a clear divergence and do not even cross for $N=900$. For $N=\bar{n}(t_{tot})=4300$, the critical radius (at the crossing of the curves subtended by the empty squares and full triangles) is much smaller than the value inferred from Fig. 6(a). The consequences of such a graphical analysis are also apparent in the left part of Fig. 10, which displays the evolution of branch widths for different cluster sizes. The absence of crossing point for $N=900$ (see Fig. 9) prevents any ramification and favors the spherical shape. This situation also occurs for smaller sizes ($N=300,420$). In the case of larger sizes ($N=2400,3000,3600$), it could be shown that the coalescence and collision time curves actually cross during the growth but without clear divergence, just like for $N=\bar{n}(t_{tot})=4300$ in Fig. 9. The crossing points are detected for sizes that are close to one other but smaller than r_c, the experimental half branch width. This accounts well for the evolution of their branch widths in the left part of Fig. 10. The clusters begin to grow as spheres up to a maximum radius which is therefore smaller than r_c. Beyond that point, the coalescence times are not significantly larger than the collision time intervals. The neck growth can continue, which explains that the branch widths are not uniform and even increase. Obviously, the morphology of platinum clusters of various sizes cannot be correctly reproduced in the case of gas phase growth if the parameter $A(T)$ is set constant. This contradicts the rough statistical description depicted in Fig. 6(a). A *sharper* divergence between coalescence and collision interval times before the termination of growth is required for a better agreement between experiment and theoretical predictions.

In growth sequences as defined in Appendix B, there are few collision events on the average. The time interval Δt_{col}^i calculated between successive collisions on a growing particle certainly underestimates the time interval $\Delta t_{col}^{i^*}$ between

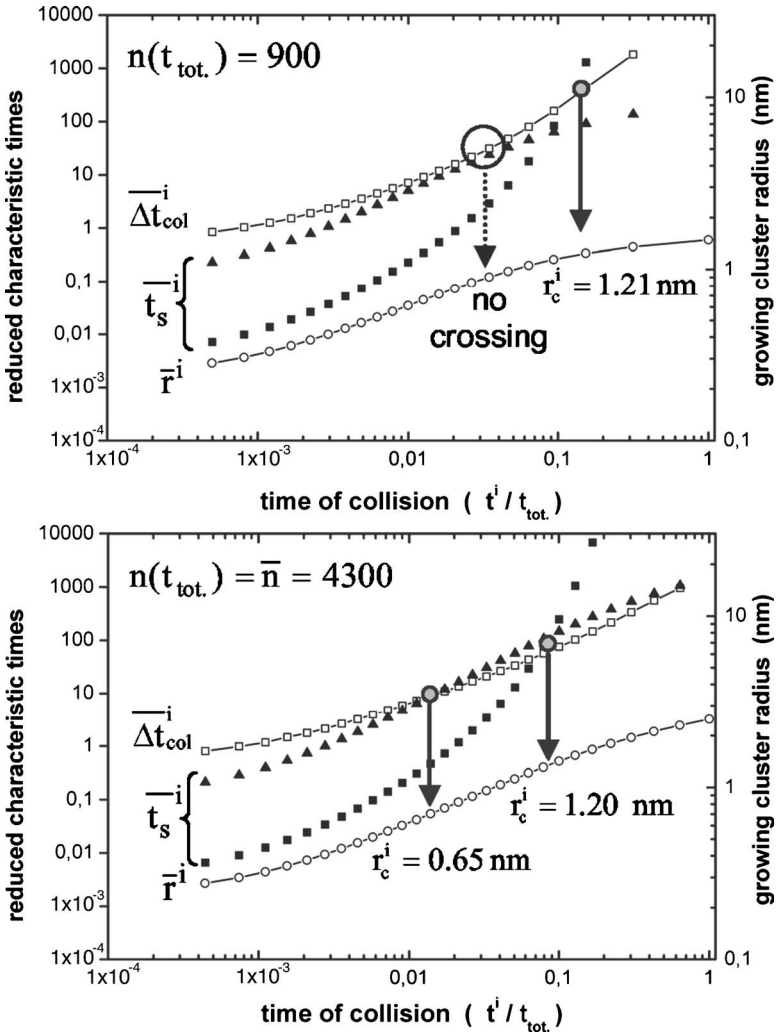

FIG. 9. Average sequences for the formation of platinum clusters containing $N=900$ atoms (top) and $N=4300$ atoms (bottom) in the case of a gas phase growth. The average characteristic times for collision (□) and coalescence (▲ and ■), and the average equivalent radius of the growing island (○) are plotted as a function of the reduced times of sticking collisions. The value of the final cluster radius at $t_i/t_{tot}=1$ is also reported. The characteristic times are normalized by the characteristic average collision time $\Delta t_{col}(t=0)$ from Fig. 6(a). The full triangles (▲) and squares (■) indicate the coalescence times calculated for isothermal growth $[A(T)/t_{tot}=A/t_{tot}=3.310^{-2}\ \mathrm{nm}^{-4}]$ or growth in a strongly cooled vapor $[A(T)/t_{tot}=10^{-3}\exp(t/\tau_{cool})\ \mathrm{nm}^{-4}]$ respectively. The critical radii at the onset of ramification are located at the intersections between $\bar{\Delta}t^i_{col}$ and $\bar{t}^i_s$ curves. For $N=900$ and isothermal growth, the crossing is avoided.

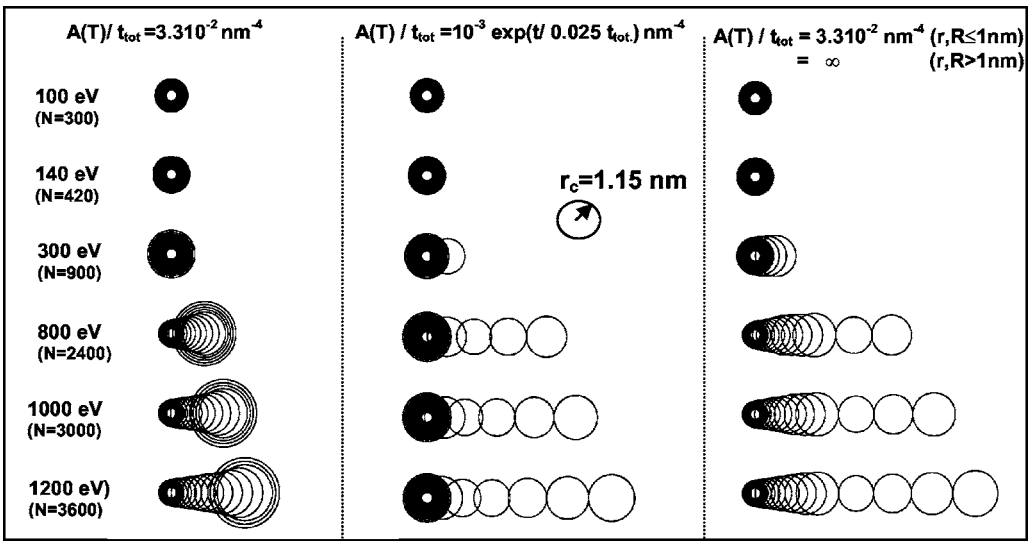

FIG. 10. Calculated evolution of the branch width of platinum clusters with an increasing number of atoms and for three different expressions of the $A(T)$ parameter in relation (3): growth at constant temperature (left), growth with a cooling rate (middle), and growth at constant temperature with a frozen coalescence above a critical radius ($r_f=1$ nm here) (right). The experimental branch width from Fig. 2 is illustrated by the $r_c=1.15$ nm radius sphere.

collisions in a more localized region of its surface and that should be considered for a comparison with coalescence dynamics (Sec. IV B). This difference is increasing in the course of growth due to the concomitant island size enlargement but is probably not significant enough to question the requirement of a marked difference between the curve slopes for both characteristic times. Moreover, considering ramified instead of spherical cluster shapes for calculating the collision kernels would have led to shorter collision time values so as to minimize this effect.[12]

A first solution for inducing a magnified divergence between collision and coalescence times could be an increase in cluster collision rates by suitably modifying the SPD parameters (Appendix A). However, this cannot be achieved without also modifying the final size distribution, in disagreement with the experiment. A more efficient explanation is to invoke a *slowing down* of coalescence rates during the growth. This may essentially originate from two mechanisms that can affect the coefficient $A(T)$ in relation (3). For a coalescence driven by surface diffusion,

$$A(T) = \zeta \frac{T}{\gamma(T) D(T)}, \tag{4}$$

where ζ is independent of T, $\gamma(T)$ is the surface tension and $D(T)$ is the surface diffusion coefficient.[13,31] Surface diffusion is a thermally activated process and its exponential temperature dependence is described by an Arrhenius law[23,32–34]

$$D(T) = D_o \exp(-E_a/kT), \tag{5}$$

where E_a is an activation energy.

If the condensing vapor is cooled during its expansion (from the target up to the source nozzle), a lengthening of the characteristic coalescence times can be roughly mimicked by writing the parameter $A(T)$ in the form $A(T)=A\exp(t/\tau_{cool})$ if the cooling rate is linear (τ_{cool} is a characteristic cooling time). The values $A/t_{tot}=10^{-3}$ nm^{-4} and $\tau_{cool}=0.025t_{tot}$ were adjusted to obtain crossing points about $r_c=1.15-1.2$ nm whatever the size considered (curves subtended by empty and black squares in Fig. 9). Since the growth kinetics is less temperature dependent than the coalescence dynamics,[12] the island growth will be assumed to occur under isothermal conditions. The corresponding results are pictured in the central part of Fig. 10 where the calculated cluster envelopes for increasing sizes show a rather constant branch width of the order of the diameter ($2r_c \cong 2.3$ nm) of the largest spherical clusters ($N=420$). These shapes are consistent with the experimental observations of Fig. 2. Other choices for A and τ_{cool} values can also bring the critical size close to r_c but the uniformityof branch widths is not reproduced so correctly. Keeping $A/t_{tot}=10^{-3}$ nm^{-4}, we have checked that the branch width of ramified clusters increases with τ_{cool} but remains almost independent of their size.

The second hypothesis for a marked slowing down of coalescence is to invoke a change in cluster morphology as a liquid-to-solid phase transition for instance. Combe *et al.* have clearly shown that the development of crystalline facets increases the characteristic time of cluster shape relaxation.[35] The atomic surface diffusion is not frozen but the particle coarsening requires that nucleation proceeds further on facets. This process is slow because of a low probability for attaching nucleation germs on these regular and flat regions. Here, the temperature is also a central parameter that rules cluster ramification. The temperature of fusion (T_f) is known to decrease as the cluster size decreases and to be almost inversely proportional to the radius.[36,37] The size of colliding clusters or the curvature radius of the growing island may reach a limiting value r_f such as the relation $T_f(r_f)=T(t_c)$ is fulfilled at a time t_c before the end of the growth sequence. The consequences of such a hypothesis have been investigated by assuming that $A(T)$ becomes infinite as soon as the radius of any of both colliding particles is larger than a particular r_f value. In the other cases, it remains constant with the previous value $A(T)/t_{tot}=3.310^{-2}$ nm^{-4}. This limits or even inhibits a further shape relaxation as illustrated in the right part of Fig. 10 where the resulting cluster shapes are drawn for $r_f=1$ nm. As compared to the first scenario (central part of Fig. 10), the overall cluster shape is less regular but the cluster morphology is only dependent on a single adjustable parameter (radius r_f).

Molecular dynamics simulations have highlighted the deficiencies of macroscopic sintering theories for describing nanocluster melting or coalescence.[38,39] An initial phase of very rapid approach is followed by a slow transformation into a single spherical entity driven by surface atomic diffusion mechanisms, much slower than predicted from macroscopic theories. Elastic and plastic deformations are prevailing during the first stage that comes to an end when the cluster pair becomes crystallized and more rigid. This discontinuity in the coalescence process is expected to be governed by the solid or liquid nature of the joined system and of both clusters before attachment. This description strengthens the hypothesis that the coalescence dynamics is sensitive to a change in the growing cluster's internal structure rather than a mere change in the temperature of the heat bath.

In every case, the final cluster morphology is sensitive to the thermodynamic properties of the constituting element. Figure 11 shows the qualitative shape evolution with size for indium, gold, and platinum particles grown under similar conditions. Depending on the element, large particles are spherical, elongated, and highly ramified respectively. This is consistent with the properties of these metals. The bulk melting temperature and the surface tension increase[40] when going from indium to platinum. The activation energy E_a for surface atomic diffusion in Eq. (5) is expected to follow the same trend. The dependence of parameter $A(T)$ [Eq. (4)] with the element will be mainly ruled by $D(T)$ [Eq. (5)] because of its exponential dependence with E_a. For a given cluster size, the characteristic times for coalescence will become longer when going from indium to platinum. Indium clusters are not large enough to display the onset of a deformation, but the shape of ellipsoidal gold particles in Fig. 11 is consistent with a branch width $2r_c$ of about 4 nm which is larger than for platinum. An explanation in terms of a phase transition effect would have been strengthened if the melting temperatures of platinum and gold clusters with respective diameters $d_c=2.5$ nm and $d_c=4$ nm were actually close one to each other. Unfortunately, quantitative estimations of the

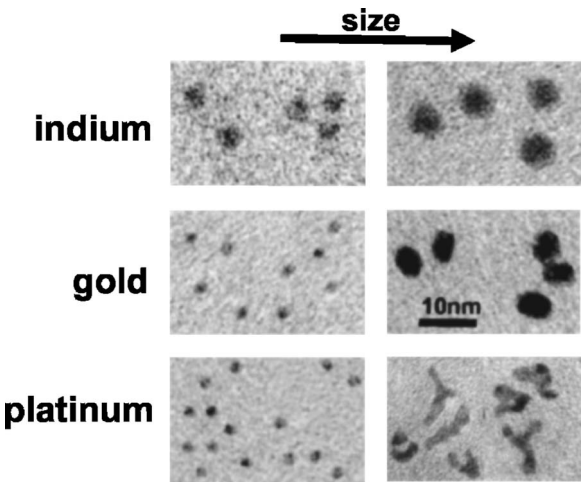

FIG. 11. Qualitative changes in the cluster morphology from small to large sizes in the case of indium, gold, and platinum. Large clusters have a 1200 eV kinetic energy and small ones are selected at 140 eV except for indium (300 eV). Their velocity is about 570 m/s^{-1} in every case.

cluster melting temperatures in the small diameter range (<10 nm) are not reliable enough to conclude in this sense.[37]

V. CONCLUSION

Thanks to size selectivity, this study has shown that large clusters produced in a laser vaporization source result from a coagulation process and are not necessarily compact (spherical). As illustrated in the case of platinum clusters, coagulation actually favors the development of ramified structures whose skeleton partly retains the memory of the way the constituting subunits were juxtaposed. Considering the general issue of the morphology of clusters grown in the gas phase, the present work confirms the major role played by the competition between the enlargement of a particle through collisions and its shape relaxation.

Coincidence between the characteristic times for coalescence and for cluster attachment proves to be an essential condition for observing ramified particles. Most of the previous models used to describe the ramification process only provide qualitative information about the morphology of particles (size averaged branch widths for instance). We have developed a more informative method for describing the average growth sequences of size-selected clusters. It shows that the apparent constancy of the branch widths observed in the present study can be explained by a strong slowing down of the surface atomic diffusion. Since this is a thermally activated process, it can be inhibited by a sudden cooling of the cluster matter. On the other hand, the development of facets when large colliding clusters turn to crystallize may give similar results. Several theoretical studies have clearly shown the importance of the onset of crystallization in relation to the dynamics of particle coarsening and rather support the second hypothesis.[16,35] In the framework of our experiment, deciding between both mechanisms requires checking the influence of external parameters on the kinetics of growth. For instance, the cooling mechanism should be very sensitive to the source operating parameters (laser power, gas pressure, nozzle diameter, etc.). Unfortunately, it was not possible to modify the experimental settings, and therefore the growth conditions, over a significantly large range for this purpose.

In a laser vaporization source, the growth involves different states of charge for the particles and experimental observations concern charged clusters, though they are much less abundant than neutral ones. The thermodynamics of the plasma plume, the specificity of charged particles as compared to neutral species should be considered for a better description.[41] It must also be recognized that the basic assumptions underlying the kinetics of growth in the framework of the Brownian coagulation model do not account for the large complexity of phenomena that actually drive the formation of clusters in a laser vaporization source. In spite of these limitations, the conclusions of this study remain quite general.

The observation of size-selected particles trapped on a surface can be a tool to investigate more systematically the mechanisms of growth in the cluster source as a function of key parameters such as the size, the bulk properties (melting temperature, surface diffusion), and the source temperature. For instance, a controlled thermal annealing of cluster in the gas phase prior to deposition is a mean to compact them into spherical particles[13] and then to infer their threshold melting temperature if it is larger than the substrate one.

APPENDIX A: THE SELF-PRESERVING SIZE DISTRIBUTION

When the number of atoms is large, it is profitable to change the discrete for a continuous variable and write the number of n atom clusters per unit volume $X_n(t)$ as $X(v,t)dv$, the cluster concentration in the size range from v to $v+dv$ ($v=nv_{at.}$ is the volume of a cluster containing n atoms with volume $v_{at.}$). Equation (A1) is written as

$$\frac{dX(v,t)}{dt} = \frac{1}{2}\int_0^v \kappa_{u,v-u}X(u,t)X(v-u,t)du - X(v,t)\int_0^\infty \kappa_{u,v}X(u,t)du. \quad \text{(A1)}$$

According to the notations of Ref. 14, the approximate resolution of these equations gives $X(v,t)=\varphi\Psi(\eta)/\bar{v}(t)^2$ where $\Psi(\eta)$ is the so-called self-preserving solution $[\int_0^\infty \Psi(\eta)d\eta=1]$ and φ is the volume of cluster matter per unit volume $[\varphi=\int_0^\infty vX(v,t)dv]$. $\bar{v}(t)=v_o(1+t/\tau_o)^{6/5}$ is the first moment (mean volume) of the cluster size distribution (v_o is the volume of the basic constituents at the initial time). $N_\infty(t)=\varphi/\bar{v}(t)=\int_0^\infty X(v,t)dv$ is the total number of particles per unit volume at time t.

The asymptotic form of $\Psi(\eta)$ (large enough t and v) is close to a log-normal distribution. For a particular choice of the collision kernels, it only depends on a single dimension-

less parameter $\eta = v/[\bar{v}(t)] = n/[\bar{n}(t)]$ but not on the starting conditions. Numerical values of $\Psi(\eta)$ are tabulated in the literature.[14] Under the hypothesis of Brownian collisions in the free molecular and isothermal regime, the kernels for spherical particles are $\kappa_{u,v} = \kappa_o (u^{1/3} + v^{1/3})^2 (\frac{1}{u} + \frac{1}{v})^{1/2}$ with $\kappa_o = (3/4\pi)^{1/6} \sqrt{6kT/\rho}$ (ρ is the material density). It turns that $1/\tau_o = \frac{5}{12} \alpha N_\infty(0) \kappa_o v_o^{1/6}$ $[\alpha = \int_0^\infty \int_0^\infty \Psi(\eta)\Psi(\eta')(\eta^{1/3} + \eta'^{1/3})(\frac{1}{\eta} + \frac{1}{\eta'})^{1/2} d\eta d\eta' \equiv 6.67$ (Ref. 14)]. For a given temperature, the final size distribution is fully characterized by two independent parameters: φ and the total time for growth t_{tot}. For $t \gg \tau_o$, it does not depend on the primary cluster volume v_o since $\bar{v}(t) \cong v_o (t/\tau_o)^{6/5} \cong (\frac{5}{12} \alpha \varphi \kappa_o t)^{6/5}$. v_o will be arbitrarily taken as the volume of an atom in the bulk phase ($v_{at.}$) and the mean cluster size at a time $t$will be $\bar{n}(t) = \bar{v}(t)/v_{at.} = (1 + t/\tau_o)^{6/5}$. In the study of platinum clusters, t_{tot} and φ (or τ_o) are adjusted to obtain a calculated size distribution as close as possible to the experimental one, with a maximum observed for $n_{\max} \cong 430$ atom clusters. The ratio t_{tot}/τ_o should therefore verify $\bar{n}(t_{tot}) = (1 + t_{tot}/\tau_o)^{6/5} \cong 10 n_{\max}$ owing the properties of $\Psi(\eta)$.[14] It is the only adjustable parameter if the reduced time of growth t/t_{tot} is considered instead of t.

Following A1, $\frac{1}{\tau}(v,t) = \int_0^\infty \kappa_{u,v} X(u,t) du$ is the characteristic frequency for collisions on a cluster of volume v, at time t. The instantaneous *average collision frequency* within the self-preserving distribution is

$$\frac{\bar{1}}{\tau}(t) = \frac{\int_0^\infty X(v,t) \frac{1}{\tau}(v,t) dv}{\int_0^\infty X(v,t) dv}$$

and reduces to

$$\frac{\bar{1}}{\tau}(t) = \frac{12}{5} \frac{1}{\tau_o} \left(\frac{\bar{v}(t)}{v_o} \right)^{-5/6}.$$

The instantaneous *average time interval* between successive collisions is defined as

$$\Delta t_c^{\mathrm{SPD}}(t) = \left(\frac{\bar{1}}{\tau}(t) \right)^{-1} = \frac{5}{12} \tau_o \left(\frac{\bar{v}(t)}{v_o} \right)^{5/6}. \tag{A2}$$

APPENDIX B: CALCULATION OF AVERAGE GROWTH SEQUENCES

We consider here the cluster volumes (instead of the number of atoms) and treat them as continuous variables for convenience, according to the notations of Appendix A. At the end of growth (time t_{tot}), a cluster with volume $\mathcal{V}$ resulting from *at least* N_c collisions at times t_i ($i = 1$ to N_c with $t_i < t_{i+1}$ and $t_{N_c+1} = t_{tot}$) can be expressed in the form

$$C_{\mathcal{V}}(t_{tot}) = C_{\mathcal{V}_1}(t_1) \oplus c_{v_1}(t_1) \oplus c_{v_2}(t_2) \oplus \cdots \oplus c_{v_{N_c-1}}(t_{N_c-1}) \oplus c_{v_{N_c}}(t_{N_c}), \tag{B1}$$

with $\mathcal{V} = \mathcal{V}_1 + \Sigma_{j=1}^{N_c} v_j$, where $C_{\mathcal{V}_1}(t_1)$ is the primary particle existing at the starting time of the sequence and around which successive c_{v_i} will agglomerate to build $C_{\mathcal{V}}(t_{tot})$.

It must be noted that t_1 is not the time of the very first collision involved in the growth of $C_{\mathcal{V}}(t_{tot})$ but rather the time of the *last but* $(N_c - 1)$ or in other terms the *first of the last* N_c constituting collisions that we are interested in. After a collision at t_i, the growing cluster that will undergo a next collision at t_{i+1} can be expressed in the recursive form

$$C_{\mathcal{V}_{i+1}}(t_{i+1}) = c_{v_i}(t_i) \oplus C_{\mathcal{V}_i}(t_i), \tag{B2}$$

with $\mathcal{V}_{i+1} = v_i + \mathcal{V}_i$, $\mathcal{V}_i = \mathcal{V}_1 + \Sigma_{j=1}^{i-1} v_j$, and $\mathcal{V}_{N_c+1} = \mathcal{V}$.

Cut back to its N_c final steps, the growth sequence of $C_{\mathcal{V}}(t_{tot})$ is fully characterized by a $\{t_i, v_i\}$ (or $\{t_i, \mathcal{V}_i\}$) data set for $i = 1$ to N_c $[\mathcal{V} = \mathcal{V}_1 + \Sigma_{j=1}^{N_c} (\mathcal{V}_{j+1} - \mathcal{V}_j)]$. A characteristic collision time interval about the time t_i can be defined as $\Delta t_{col}^i = t_{i+1} - t_i$. All these notations apply to gas phase growth as well as surface growth in deposition experiments with a preformed cluster beam. We differentiate the smallest and largest partners in a collision process by labelling them the *colliding* (or primary) *cluster* c_{v_i} and the *growing island* $C_{\mathcal{V}_i}$, respectively. This is a natural choice in the case of cluster film formation on surfaces where the growing particles are motionless. In the gas phase, this amounts to consider that the center of mass of the growing particle of interest is arbitrarily located on the largest colliding particle.

A $C_{\mathcal{V}}$ cluster can result from any of growth sequences as illustrated by (B1) and an average growth sequence is obtained by weighting each of them with their respective probability so as to write

$$C_{\mathcal{V}}^{av.}(t_{tot}) \equiv C_{\bar{\mathcal{V}}_1}(\bar{t}_1) \oplus c_{\bar{v}_1}(\bar{t}_1) \oplus c_{\bar{v}_2}(\bar{t}_2) \oplus \cdots \oplus c_{\bar{v}_{N_c-1}}(\bar{t}_{N_c-1}) \oplus c_{\bar{v}_{N_c}}(\bar{t}_{Nc}),$$

where $\bar{v}_i$ and $\bar{t}_i$ are respectively the average volume of the colliding cluster and the average time of occurrence for the ith of the last N_c collision steps under consideration ($\bar{\mathcal{V}}_1 = \mathcal{V} - \Sigma_{i=1}^{N_c} \bar{v}_i$). The probability for a cluster $C_{\mathcal{V}_{i+1}}(t_{i+1})$ to result from the process (B2) that occurs in the t_i to $t_i + dt_i$ time range and involves a growing island with a volume in the range from $\mathcal{V}_i$ to $\mathcal{V}_i + d\mathcal{V}_i$ is

$$p(\mathcal{V}_i, t_i; \mathcal{V}_{i+1}, t_{i+1}) dt_i d\mathcal{V}_i = \frac{X(\mathcal{V}_{i+1} - \mathcal{V}_i, t_i) \cdot X(\mathcal{V}_i, t_i)}{X(\mathcal{V}_{i+1}, t_{i+1})} \cdot \kappa_{\mathcal{V}_{i+1} - \mathcal{V}_i, \mathcal{V}_i} \cdot \exp\left\{ - \int_{t_i}^{t_{i+1}} \left[\int_0^\infty \kappa_{u, \mathcal{V}_{i+1}} X(u,t) du \right] dt \right\} \cdot dt_i d\mathcal{V}_i$$

The exponential term represents the probability for a cluster with volume $\mathcal{V}_{i+1}$ born at time t_i to survive till time t_{i+1}. Since $\mathcal{V}_i$ is defined as the volume of the largest of both colliding clusters (v_i and $\mathcal{V}_i$), double counting is avoided by setting $\mathcal{V}_i \geqslant \mathcal{V}_{i+1} - \mathcal{V}_i$. It can then be checked that

$$\int_0^{t_{i+1}} \int_{\frac{\mathcal{V}_{i+1}}{2}}^{\mathcal{V}_{i+1}} p(\mathcal{V}_i,t_i;\mathcal{V}_{i+1},t_{i+1})dt_i d\mathcal{V}_i = 1$$

as soon as $X(\mathcal{V}_{i+1},0) \cong 0$ which is true if $\mathcal{V}_{i+1}$ is larger than v_o (Appendix A). The density of probability for the whole sequence (B1) is

$$p^{N_c}(\{\mathcal{V}_i,t_i\}) = \prod_{\alpha=1}^{N_c} p(\mathcal{V}_\alpha,t_\alpha;\mathcal{V}_{\alpha+1},t_{\alpha+1}) \tag{B3}$$

and verifies

$$\int_0^{t_{N_c+1}=t_{tot}} \int_{\frac{\mathcal{V}_{N_c+1}}{2}}^{\mathcal{V}_{N_c+1}=\mathcal{V}} dt_{N_c} d\mathcal{V}_{N_c} \cdots \left\{ \int_0^{t_{j+1}} \int_{\frac{\mathcal{V}_{j+1}}{2}}^{\mathcal{V}_{j+1}} dt_j d\mathcal{V}_j \cdots \left[\int_0^{t_3} \int_{\frac{\mathcal{V}_3}{2}}^{\mathcal{V}_3} dt_2 d\mathcal{V}_2 \left(\int_0^{t_2} \int_{\frac{\mathcal{V}_2}{2}}^{\mathcal{V}_2} p^{Nc}(\{\mathcal{V}_i,t_i\}) dt_1 d\mathcal{V}_1 \right) \right] \right\} = 1.$$

Average volumes and times can be expressed as follows:

$$\bar{t}_j^{N_c} = \int_0^{t_{N_c+1}=t_{tot}} \int_{\frac{\mathcal{V}_{N_c+1}}{2}}^{\mathcal{V}_{N_c+1}=\mathcal{V}} dt_{N_c} d\mathcal{V}_{N_c} \cdots \left\{ \int_0^{t_{j+1}} \int_{\frac{\mathcal{V}_{j+1}}{2}}^{\mathcal{V}_{j+1}} dt_j t_j d\mathcal{V}_j \cdots \left[\int_0^{t_3} \int_{\frac{\mathcal{V}_3}{2}}^{\mathcal{V}_3} dt_2 d\mathcal{V}_2 \left(\int_0^{t_2} \int_{\frac{\mathcal{V}_2}{2}}^{\mathcal{V}_2} p^{Nc}(\{\mathcal{V}_i,t_i\}) dt_1 d\mathcal{V}_1 \right) \right] \right\}, \tag{B4}$$

$$\bar{\mathcal{V}}_j^{N_c} = \int_0^{t_{N_c+1}=t_{tot}} \int_{\frac{\mathcal{V}_{N_c+1}}{2}}^{\mathcal{V}_{N_c+1}=\mathcal{V}} dt_{N_c} d\mathcal{V}_{N_c} \cdots \left\{ \int_0^{t_{j+1}} \int_{\frac{\mathcal{V}_{j+1}}{2}}^{\mathcal{V}_{j+1}} dt_j \mathcal{V}_j d\mathcal{V}_j \cdots \left[\int_0^{t_3} \int_{\frac{\mathcal{V}_3}{2}}^{\mathcal{V}_3} dt_2 d\mathcal{V}_2 \left(\int_0^{t_2} \int_{\frac{\mathcal{V}_2}{2}}^{\mathcal{V}_2} p^{Nc}(\{\mathcal{V}_i,t_i\}) dt_1 d\mathcal{V}_1 \right) \right] \right\}, \tag{B5}$$

$$\bar{v}_j^{N_c} = \int_0^{t_{N_c+1}=t_{tot}} \int_{\frac{\mathcal{V}_{N_c+1}}{2}}^{\mathcal{V}_{N_c+1}=\mathcal{V}} dt_{N_c} d\mathcal{V}_{N_c} \cdots \left\{ \int_0^{t_{j+1}} \int_{\frac{\mathcal{V}_{j+1}}{2}}^{\mathcal{V}_{j+1}} dt_j v_j d\mathcal{V}_j \cdots \left[\int_0^{t_3} \int_{\frac{\mathcal{V}_3}{2}}^{\mathcal{V}_3} dt_2 d\mathcal{V}_2 \left(\int_0^{t_2} \int_{\frac{\mathcal{V}_2}{2}}^{\mathcal{V}_2} p^{Nc}(\{\mathcal{V}_i,t_i\}) dt_1 d\mathcal{V}_1 \right) \right] \right\}, \tag{B6}$$

with $\bar{v}_j^{N_c} = \bar{\mathcal{V}}_{j+1}^{N_c} - \bar{\mathcal{V}}_j^{N_c}$.

The index N_c, omitted before, is necessary to identify the collision sequence through its minimum number of steps. From the properties of $p^{Nc}(\{\mathcal{V}_i,t_i\})$ [Eq. (B3)], it is straightforward to check that the first $(j-1)$ integrals can be reduced to unity in such a way that

$$\bar{\mathcal{V}}_j^{N_c} = \bar{\mathcal{V}}_1^{N_c-(j-1)},$$

$$\bar{v}_j^{N_c} = \bar{v}_1^{N_c-(j-1)},$$

and

$$\bar{t}_j^{N_c} = \bar{t}_1^{N_c-(j-1)}.$$

The average volume of the growing island at the jth of the last N_c collision steps is the same as the average initial volume in a collision sequence having at least $N_c-(j-1)$ steps.

A data set $\{\bar{t}_i, \bar{\mathcal{V}}_i\}^{N_c^{\max}}$ is then obtained by calculating $\bar{\mathcal{V}}_1^{N_c}$ and $\bar{t}_1^{N_c}$ from relations (B4) and (B5) through a recursive procedure where N_c is varied from 1 to $N_c^{\max}$. Since the SPD approximation is not valid for the earliest times of growth, we only consider the latter collision steps and the upper limit $N_c^{\max}$ is arbitrarily chosen so that the initial clusters (volume $\bar{\mathcal{V}}_1^{N_c^{\max}}$) contain six to seven atoms at a maximum. In Figs. 7 and 9, the quantities $\Delta\bar{t}_{col}^i = \bar{t}_{i+1}^{N_c^{\max}} - \bar{t}_i^{N_c^{\max}}$ and $\bar{r}^i = \sqrt[3]{3\bar{\mathcal{V}}_i^{N_c^{\max}}/4\pi}$ are reported as a function of the reduced collision times $t_i/t_{tot} = \bar{t}_i^{N_c^{\max}}/t_{tot}$. The coalescence times $\bar{t}_s^i$ are calculated from relation (3), $\bar{t}_s^i = A(T)(\bar{r}^i \cdot \bar{r}_o^i)^2$, where $\bar{r}^i = \sqrt[3]{3\bar{\mathcal{V}}_i^{N_c^{\max}}/4\pi}$ is the radius of the growing island (B5) and $\bar{r}_o^i = \sqrt[3]{[3\bar{v}_i^{N_c^{\max}}/4\pi]} = \sqrt[3]{[3(\bar{\mathcal{V}}_{i+1}^{N_c^{\max}} - \bar{\mathcal{V}}_i^{N_c^{\max}})/4\pi]}$ is the radius of the colliding cluster (B6).

*E-mail address: pellarin@lasim.univ-lyon1.fr

[1] R. T. Laaskonen, D. A. Goetsch, D. W. Owens, D. M. Poirier, F. Stepniak, J. H. Weaver, Rev. Sci. Instrum. **65**, 2267 (1994).

[2] Bu. Wrenger and K. H. Meiwes-Broer, Rev. Sci. Instrum. **68**, 2027 (1997).

[3] B. von Issendorf and R. E. Palmer, Rev. Sci. Instrum. **70**, 4497 (1999).

[4] P. M. Denby and D. A. Eastham, Nucl. Instrum. Methods Phys. Res. A **441**, 588 (2000).

[5] R. Alayan, L. Arnaud, A. Bourgey, M. Broyer, E. Cottancin, G. Guiraud, J. R. Huntzinger, J. Lermé, J. L. Vialle, and M. Pellarin, Rev. Sci. Instrum. **75**, 2461 (2004).

[6] J. M. Soler, N. Garcia, O. Echt, K. Sattler, E. Recknagel, Phys. Rev. Lett. **49**, 1857 (1982).

[7] T. P. Martin, Phys. Rep. **273**, 199 (1996).
[8] M. Pellarin, B. Baguenard, J. L. Vialle, J. Lermé, M. Broyer, J. Miller, andA. Pérez, Chem. Phys. Lett. **217**, 349 (1994).
[9] F. F. Abraham, *Homogeneous Nucleation Theory* (Academic, New York, 1974).
[10] F. Baletto and R. Ferrando, Rev. Mod. Phys. **77**, 371 (2005).
[11] C. G. Granqvist and R. A. Buhrman, J. Appl. Phys. **47**, 2200 (1976); , Solid State Commun. **18**, 123 (1976).
[12] R. C. Flagan and M. M. Lunden, Mater. Sci. Eng., A **204**, 113 (1995).
[13] D. L. Olynick, J. M. Gibson, and R. S. Averback, Philos. Mag. A **77**, 1205 (1998).
[14] F. S. Lai, S. K. Friedlander, J. Pich, and G. M. Hidy, J. Colloid Interface Sci. **39**, 395 (1972).
[15] K. E. J. Lehtinen and M. R. Zachariah, J. Colloid Interface Sci. **242**, 314 (2001).
[16] R. Meyer, J. J. Gafner, S. L. Gafner, S. Stappert, B. Rellinghaus, and P. Entel, Phase Transitions **78**, 35 (2005).
[17] U. Kreibig and M. Vollmer, *Optical Properties of Metal Clusters* (Springer, New York, 1995), and references therein.
[18] D. E. Clemmer and M. F. Jarrold, J. Mass Spectrom. **32**, 577 (1997).
[19] S. Stappert, B. Rellinghaus, M. Acet, E. F. Wassermann, J. Cryst. Growth **252**, 440 (2003).
[20] P. Mélinon, V. Paillard, V. Dupuis, A. Pérez, P. Jensen, A. Hoareau, J. P. Pérez, J. Tuaillon, M. Broyer, J. L. Vialle, M. Pellarin, B. Baguenard, and J. Lermé, Int. J. Mod. Phys. B **9**, 339 (1995).
[21] C. Kittel, *Introduction to Solid State Physics* (Wiley, New York, 1976).
[22] M. von Smoluchowski, Z. Phys. Chem., Stoechiom. Verwandtschaftsl. **92**, 129 (1917).
[23] P. Jensen, Rev. Mod. Phys. **71**, 1695 (1999).
[24] L. Bardotti, P. Jensen, A. Hoareau, M. Treilleux, and B. Cabaud, Phys. Rev. Lett. **74**, 4694 (1995).
[25] B. Yoon, V. Akulin, Ph. Cahuzac, F. Carlier, M. de Frutos, A. Masson, C. Mory, C. Colliex, and C. Bréchignac, Surf. Sci. **443**, 76 (1999).
[26] W. D. Kingery, J. Appl. Phys. **31**, 833 (1960).
[27] Cluster attachment is an exothermic reaction and the temperature increases after each collision. This local temperature should be considered with regard to coalescence dynamics. Here, we assume that formed clusters rapidly cool down by collisions with the background gas (or interaction with the substrate) and reach quasi-instantaneously the equilibrium temperature. This hypothesis is all the more valid since the larger the colliding clusters, the smaller the relative increase in temperature.
[28] A. A. Lushnikov, J. Colloid Interface Sci. **45**, 549 (1973).
[29] S. H. Park, F. E. Kruis, K. W. Lee, and H. Fissan, Aerosol Sci. Technol. **36**, 419 (2002).
[30] A. Prakash, A. P. Bapat, and M. R. Zachariah, Aerosol Sci. Technol. **37**, 892 (2003).
[31] F. A. Nichols, J. Appl. Phys. **37**, 2805 (1966).
[32] S. Arcidiacono, N. R. Bieri, D. Poulikakos, and C. P. Grigoropoulos, Int. J. Multiphase Flow **30**, 979 (2004).
[33] I. Yokoyama, Physica B **271**, 230 (1999).
[34] Y. G. Chushak and L. S. Bartell, J. Phys. Chem. B **105**, 11605 (2001).
[35] N. Combe, P. Jensen, and A. Pimpinelli, Phys. Rev. Lett. **85**, 110 (2000).
[36] P. Buffat and J. P. Borel, Phys. Rev. A **13**, 2287 (1976).
[37] M. Wautelet, J. Phys. D **24**, 343 (1991).
[38] H. Zhu and R. S. Averback, Philos. Mag. Lett. **73**, 27 (1996).
[39] L. J. Lewis, P. Jensen, and J. L. Barrat, Phys. Rev. B **56**, 2248 (1997).
[40] *Handbook of Chemistry and Physics*, edited by D. R. Lide, 80th ed. (CRC, Cleveland, 1999).
[41] R. B. Huang, Q. Zhang, H. Chen, and L. S. Zheng, Eur. Phys. J. D **9**, 253 (1999).